npj | climate and atmospheric science

Article

Published in partnership with CECCR at King Abdulaziz University

https://doi.org/10.1038/s41612-025-01317-0

Strengthening of favorable environments for North Atlantic tropical cyclogenesis in midlatitudes in a warmer climate

A. Montoro-Mendoza[1,2] ✉, C. Calvo-Sancho[3], J. J. González-Alemán[4], J. Díaz-Fernández[1,5], P. Bolgiani[5] & M. L. Martín[1,6]

Anthropogenic climate change is intensifying tropical cyclones, and some studies suggest that they are now impacting regions farther from the equator, though uncertainties remain. This study examines the North Atlantic (NATL) basin's autumn climatology, focusing on environments conducive to tropical transitions (TTs), as most cyclones affecting Europe that originate from TTs occur during this season. Ten CMIP6 climate models under the historical, SSP2-4.5 and SSP5-8.5 scenarios are used, covering the 1981–2100 period, with the ERA5 reanalysis employed as a reference to support the results. The study introduces the Tropical Transition Favorability Index (TTFI), which is a novel metric that integrates key parameters to quantify environmental favorability for TTs in the NATL. Findings indicate a progressive tropicalization of the NATL basin under both SSP2-4.5 and SSP5-8.5, with a more pronounced effect under the latter, driven by increased sea surface temperatures and humidity, while dynamic constraints weaken. Although in some cases the magnitude of projected future changes is comparable to existing CMIP6 models biases with respect to ERA5, the results suggest a higher likelihood of TTs, increasing the risk from these destructive systems.

Patterns in TCs activity are highly important to society. The destructive effects of TCs have posed significant challenges for the economies and societies of the affected nations[1–5]. A TC is a synoptic low-pressure system with a warm core and organized deep convection, characterized by a non-frontal structure, which typically forms over tropical and subtropical latitudes[6]. TCs commonly have a barotropic origin[7]. Nonetheless, when favorable baroclinic atmospheric conditions are present, a series of precursor disturbances may contribute to the formation of TCs[6,8]. Tropical transitions (TTs) in the North Atlantic (NATL) basin represent a critical pathway for the development of TCs from extratropical or subtropical disturbances under favorable conditions[6,9]. This process is historically associated with a process of rapid cyclogenesis, where a midlatitude baroclinic system transform into a TC as it interacts with favorable atmospheric conditions, such as warm sea surface temperature (SST), decreased stability and high lower-troposphere moisture content[10,11], resulting in a decrease in wind shear[12] and redistribution of potential vorticity due to the large quantity of latent heat released in the moments previous to a TT occurrence[7,8,10,12–14].

TTs development in the NATL basin is significantly influenced by several atmospheric and oceanic parameters. Firstly, the SST plays a crucial role in the intensity of TCs in the NATL basin[15–17]. Warm SST, typically above 25.5 °C at mid-latitude regions[18], provides the necessary heat and moisture to fuel TCs, enabling their development and intensification. During a TT, the pre-existing baroclinic systems rely on warm SST to provide the latent heat necessary for the transition[10]. These conditions encourage the development of a low-level warm-core structure, which is essential for a system to be classified as tropical. Moreover, the above-mentioned threshold of 25.5 °C not only supports the genesis of TCs but also could enhance the efficiency of TTs by reducing thermal disequilibrium between the ocean and atmosphere[19]. Studies such as Pérez-Alarcón et al.[17] highlight that a warmer SST enhances atmospheric instability and moisture availability, as remarked by Knutson et al.[20], who emphasize the critical role of warmer SST in intensifying the hydrological cycle. Therefore, the increasing moisture availability due to higher SST values enables the transformation of mid-latitude cyclones or other disturbances into tropical systems. The total column water (TCW) is a key indicator of the

[1]Department of Applied Mathematics. Faculty of Computer Engineering, Universidad de Valladolid, Valladolid, Spain. [2]Consejo Superior de Investigaciones Científicas (CSIC). Instituto de Geociencias (IGEO), Madrid, Spain. [3]Centro de Investigaciones sobre Desertificación, Consejo Superior de Investigaciones Científicas (CIDE, CSIC-UV-GVA), Climate, Atmosphere and Ocean Laboratory (Climatoc-Lab), Moncada, Valencia, Spain. [4]Agencia Estatal de Meteorología (AEMET). Department of Development and Applications, Madrid, Spain. [5]Department of Earth Physics and Astrophysics. Faculty of Physics, Universidad Complutense de Madrid, Madrid, Spain. [6]Interdisciplinary Mathematics Institute. Universidad Complutense de Madrid, Madrid, Spain. ✉e-mail: ana.montoro@uva.es

atmospheric moisture availability, which must be sufficiently high (typically 30 - 40 mm) to support deep convection and sustain TCs intensity[10,14,17].

Moreover, the interaction between the Coupling Index (CI) and the vertical wind shear (WSH) is key in determining the likelihood of TTs in the NATL basin. A low CI, indicative of reduced tropospheric stability, facilitates the vertical transport of heat and moisture, reducing the inhibition of upward motion and promoting the development of robust convective systems[7,16]. Calvo-Sancho et al.[10] expanded on these findings, confirming that CI values drop below 22.5 °C during TTs, which is an upper limit identified by McTaggart-Cowan et al.[15] However, the impact of the CI is affected by the WSH. High WSH values disrupts the vertical cyclone structure, inhibiting deep convection[7,21,22]. Therefore, tropical cyclogenesis and maintenance are favored under conditions of low CI and WSH values, as reduced tropospheric stability favors deep convection while weak WSH values prevent the tilting and disruption of the TC vortex, enabling the development of a well-organized and symmetric warm-core system. It is important to note that high WSH is indeed a necessary ingredient for TT, but mainly in the previous stages associated with extratropical or subtropical disturbances[7,10,20]. Together, these parameters provide a framework for understanding tropical cyclogenesis via mid-latitude dynamics in the NATL basin.

The occurrence and intensity of TTs, along with the environments that favor them, are increasingly of interest as these cyclones are now impacting regions farther from the equator, potentially driven by Anthropogenic Climate Change (ACC)[11,23–27]. Although several studies have reported a poleward expansion of TC activity, linked to the tropicalization (the process by which northern latitudes exhibit environmental conditions typical of tropical regions) of higher latitudes in the NATL[23,25,28], this pattern remains uncertain and may not be uniform across basins or time periods. Recent analyses even suggest a southward shift in NATL TC genesis over the past decades[29]. While the frequency of TCs has increased, this trend is accompanied by a similar decrease of weaker TCs[20,30]. Debate persists due to limitations in reanalysis data, such as the missing storms before the satellite era[5,31,32]. Nonetheless, the eastern NATL coast has recently experienced the effects of notable TCs formed through TTs, such as Ophelia in 2017 and Leslie in 2018, which reached the coasts of Europe, a rare occurrence that underscores the growing threat of intense TCs to traditionally unaffected areas[4,10,33,34]. Therefore, as global warming continues to influence those variables related to the TTs development[11,35,36], understanding TT dynamics and their changes in the NATL basin is essential, especially given the potential for more intense TCs of TT origin to reach Europe and other extratropical regions[10,14].

The current study aims to examine the climatology of the NATL environments conducive to TTs, focusing on how the ACC might impact these patterns, specifically during the autumn months (September, October, November; SON), when TTs are most likely to develop in the NATL basin[7,10,37]. Several climate models from the Coupled Model Intercomparison Project Phase 6 (CMIP6)[38] repository are used to capture the uncertainty associated, considering the historical, SSP2.4-5 and SSP5-8.5 scenarios (Shared Socioeconomic Pathways)[39]. As CMIP6 models are insufficient to examine TT events[40], this study is restricted to environmental fields, focusing on the large-scale environmental conditions that modulate TT activity rather than individual storm events. For this purpose, the climatology of those parameters related to TTs development (specified in the Methods section) is analyzed for the SON season. Additionally, a novel index indicative of environments conducive to TTs development over the NATL is here defined, which consists of the ratio of thermodynamic factors that enhance TTs to dynamic ones, which hinder TTs development. This aims to provide a more precise assessment of the environmental conditions that favor TTs development over the domain of study. The climatology of such an index is then computed and analyzed in detail, allowing for the identification of spatial and temporal patterns in TT-prone regions. Three 30-year periods sufficiently spaced in time are selected, which are the historical (1981–2010), the near future (2021–2050), and the far future (2071–2100) periods.

Results

Climatological behavior of individual parameters

To assess the similarity between the multi-model CMIP6 composite and the ERA5 reanalysis, the differences are calculated as ERA5 minus the CMIP6 multi-model mean, and are shown in all panels labeled a) in the figures of this study. The SST results indicate that the historical climatology derived from the CMIP6 selected model composite shows positive differences when compared with ERA5 (Fig. 1a), i.e., the ERA5 reanalysis displays higher values than the CMIP6 composite across most of the NATL basin. This discrepancy is particularly pronounced in the region around 50°W-35°W and 40°N-50°N, suggesting that CMIP6 models tend to underestimate SST in this area. Figure 1b presents the historical climatology of the SST, where it can be appreciated that warm SST dominates the tropical and subtropical Atlantic, with most of the regions below 30°N exceeding 25.5 °C (striped region), which is the threshold above-mentioned for TC formation[18].

Figure 1c, d show SST positive anomaly values for the near and far future periods, respectively, under the SSP2-4.5 scenario, being statistically significant across almost the whole domain. In Fig. 1e, f the increase when considering the SSP5-8.5 scenario is more accused, and the statistically significant region is wider. The anomaly patterns appreciated align with those of Fox-Kemper et al. (Fig. 9.3)[35] and Montoro–Mendoza et al.[11] The absence of negative anomalies across both projected periods suggests a widespread warming trend due to the ACC when considering both the SSP2-4.5 and the SSP5-8.5 scenarios, with warming intensifying in the late-century period. The anomalies indicate that the threshold for TC formation (typically 25.5 °C) will be met over a larger area. As warming shifts northward, it makes higher-latitude regions more conducive to tropical cyclogenesis, expanding the geographic range of tropical systems, which aligns with discussions of a poleward shift in TC tracks[20,23,25]. It is critical to note, however, that debate persists regarding the magnitude and drivers of this shift[29]. The increase in SST due to the ACC[35,41] may lead to more frequent TTs and intensification of TCs[17,42,43], expanding areas favorable for TTs development and raising risks for coastal populations.

The TCW comparison between ERA5 and the CMIP6 multi-model composite (Fig. 2a) shows a generally consistent representation of the spatial distribution and magnitude of TCW. However, some regional discrepancies emerge. In the central-western tropical Atlantic and between 60°W-40°W and 10°N-20°N, the CMIP6 models display negative differences, indicating an overestimation of CMIP6 historical TCW, relative to ERA5 (Fig. 2a). Conversely, positive differences are observed between 35°W-0°W and 10°N-25°N, where CMIP6 underestimates TCW compared to ERA5. This east-west contrast suggests that while the models broadly capture the TCW climatological pattern, they misrepresent the intensity and distribution of moisture in some regions. The highest values of historical TCW (50–60 mm) are concentrated in the tropics (Fig. 2b), particularly between 0°N and 20°N, associated with the warm, moist air of the tropical regions. Lower TCW values (10–30 mm) are observed over higher latitudes reflecting cooler, drier air typically found in extratropical regions. Figure 2c–f displays positive and statistically significant TCW anomalies across most of the domain, except for Fig. 2c, which shows some not statistically significant regions. This indicates enhanced atmospheric moisture content due to rising SST, among other factors, since it promotes increased evaporation and latent heat flux[17,19], alongside the higher capacity of air to hold more humidity as it warms. Anomalies intensify markedly in the far future period for both emission scenarios (Fig. 2d, f), with stronger signals under SSP5-8.5 (Fig. 2f) and the largest increases concentrated between 0°N and 30°N.

Although a historical global reduction in TC frequency is observed, considering the July to October months according to Zhao et al.[44], the SST and TCW anomalies shown in Figs. 1, 2 suggest that TCs may become more intense and could potentially develop further poleward, as northern regions acquire characteristics typical of environments conducive to TC intensification[43,45]. These conditions are more pronounced under SSP5-8.5 but are also evident in SSP2-4.5. The behavior of these two variables is

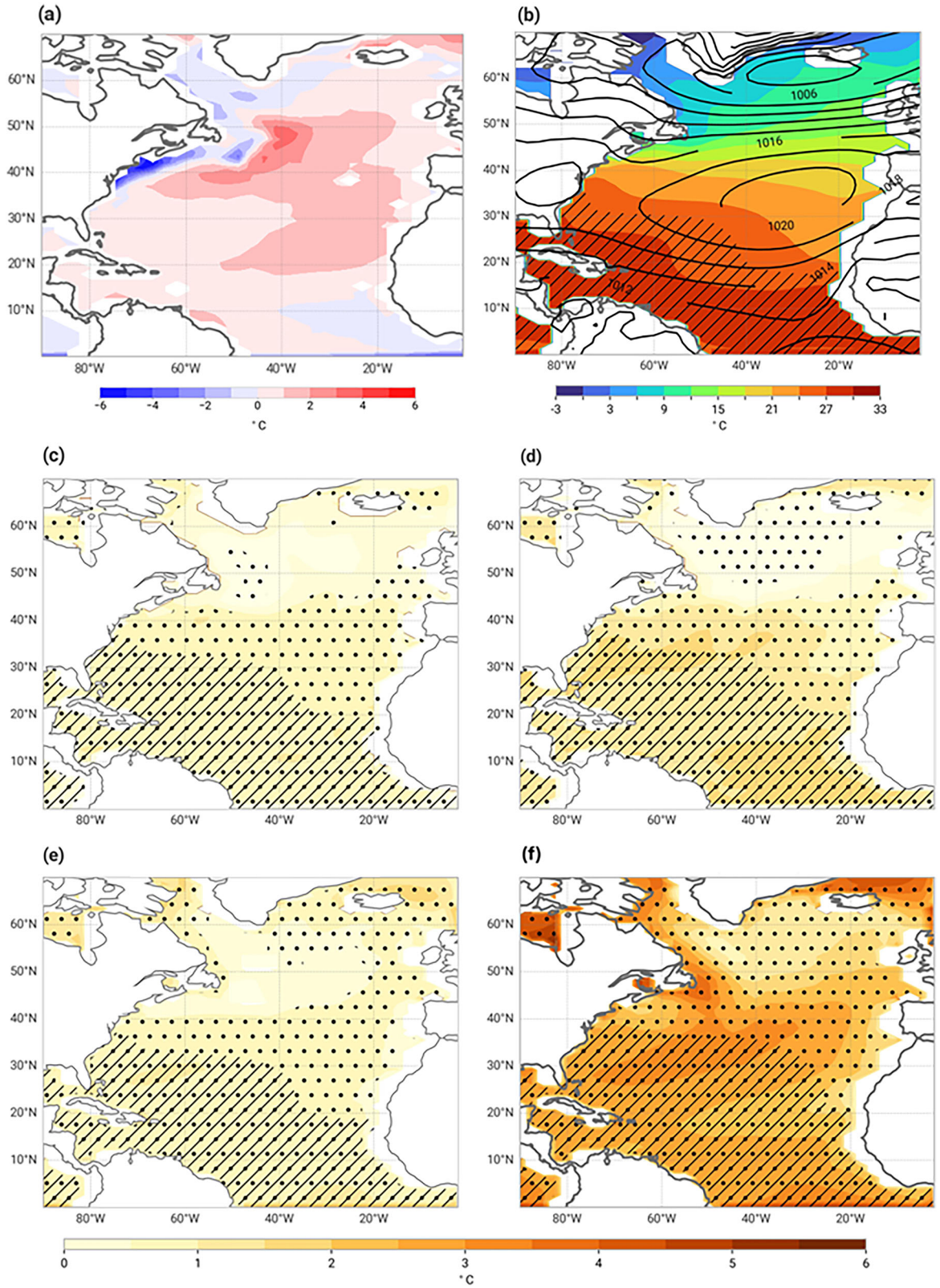

Fig. 1 | SON historical climatology, SSP2-4.5 and SSP5-8.5 projections of SST in the NATL for the XXI century. a SON ERA5 historical climatology differences of SST (°C) with respect to the multi-model CMIP6 composite. **b** SON historical climatology values from the multi-model CMIP6 composite of SST (°C) and MSLP (hPa; black contours). SON anomaly values with respect to **b** of SST (°C) for the **c** near future period and **d** far future period considering the SSP2-4.5 scenario; with respect to **b** of SST (°C) for **e** near future period and **f** far future period considering the SSP5-8.5 scenario. Black dots indicate statistically significant anomalies based on the Mann–Whitney U test ($\alpha = 0.05$). Stripped regions in (**b**) indicate where the SST value is higher or equal to 25.5 °C; in (**c**–**f**) indicate where the SST value is higher or equal to 25.5 °C, adding the anomaly value to the **b** field.

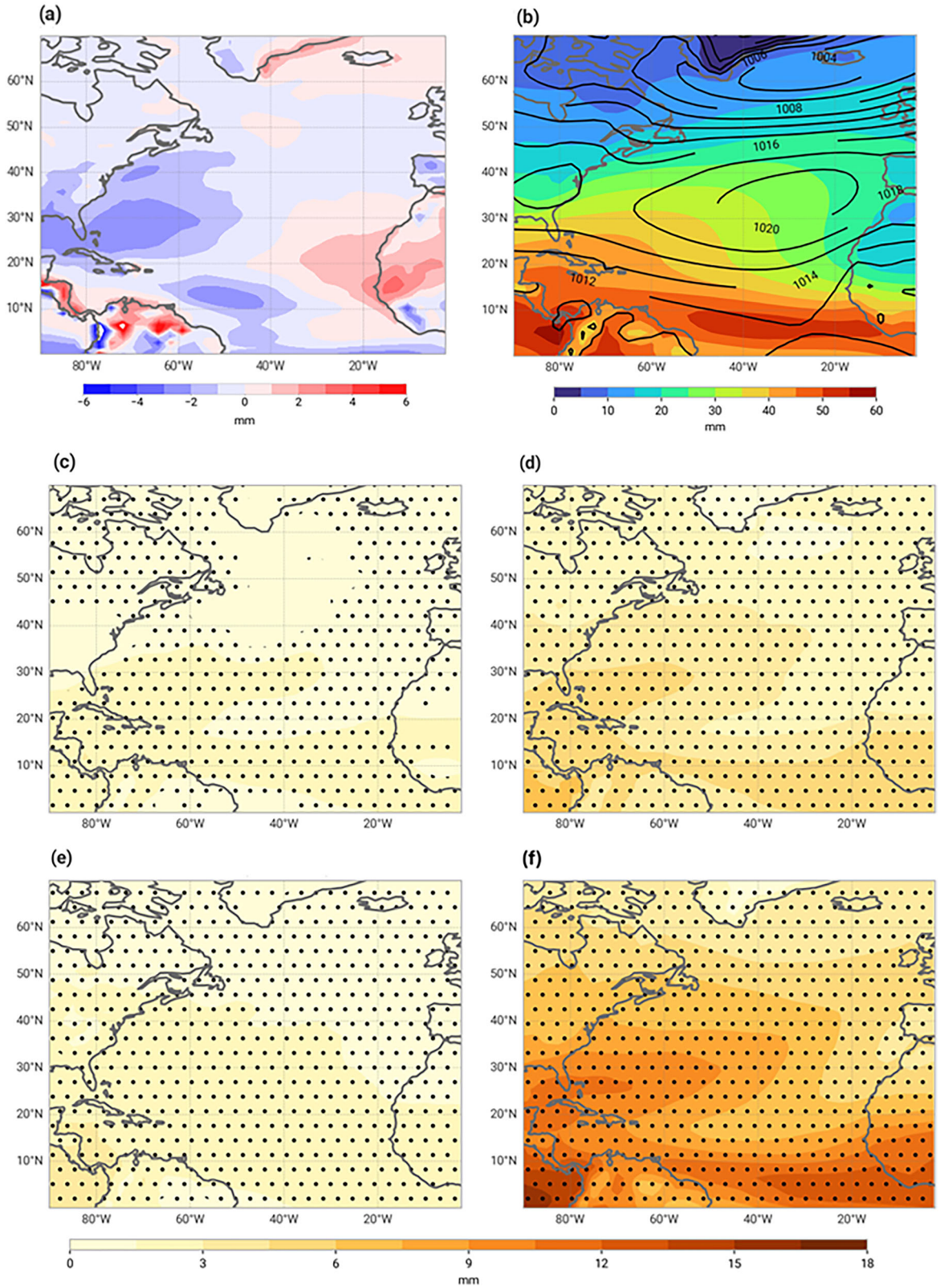

Fig. 2 | SON historical climatology, SSP2-4.5 and SSP5-8.5 projections of TCW in the NATL for the XXI century. a SON ERA5 historical climatology differences of TCW (mm) with respect to the multi-model CMIP6 composite. **b** SON historical climatology values from the multi-model CMIP6 composite of TCW (mm) and MSLP (hPa; black contours. SON anomaly values with respect to **b** of TCW (mm) for the **c** near future period and **d** far future period considering the SSP2-4.5 scenario; with respect to **b** of TCW (mm) for the **e** near future period and **f** far future period considering the SSP5-8.5 scenario. Black dots indicate statistically significant anomalies based on the Mann–Whitney U test ($\alpha = 0.05$).

consistent with previous studies[11,25,28], supporting the possibility of a poleward migration of TC activity in the NATL basin.

Other parameters may also help to analyze the environments conducive to TTs development, like WSH and CI, which play vital roles in cyclone dynamics[7,16,19]. When comparing the seasonal maximum value (max) of the WSH, considering the 850 - 250 hPa layer ($WSH_{850,250}$), historical field of ERA5 with the multi-model CMIP6 composite, the differences reveal some discrepancies (Fig. 3a). Positive differences are present over the western tropical Atlantic (90°W-70°W, 0°-25°N), the eastern tropical Atlantic (50°W-0°W, 10°-20°N), and at latitudes greater than ~50°N. This suggests that CMIP6 models may systematically underestimate max $WSH_{850,250}$ in these regions, relative to the ERA5 reanalysis. Conversely, a localized pocket of negative anomalies is observed around 50°W, 35°N, indicating an area where CMIP6 exhibits stronger max $WSH_{850,250}$ than ERA5. Elsewhere across the basin, no differences are evident, which implies general agreement between ERA5 and the multi-model composite outside of the highlighted regions. Figure 3b shows the historical climatology of the max $WSH_{850,250}$, where it can be appreciated that the maximum value is reached over the East Coast area of the United States, which aligns with Aiyyer and Thorncroft[21] and Michaelis and Lackmann[46].

Future projections reveal contrasting responses depending on the emissions pathway. Under SSP2-4.5 (Fig. 3c, d), both the near and far future periods project positive anomalies of max $WSH_{850,250}$ across the tropical Atlantic (5°-15°N) and the central-western Atlantic (10°-35°N; 90°-40°W). These anomalies strengthen toward the end of the century, consistent with Vecchi and Soden[47], who reported statistically significant increases in WSH over the same region in the NATL basin under the IPCC AR4 midrange A1B scenario. Accordingly, under SSP2-4.5, the tropical and central-western Atlantic are projected to experience persistently elevated max $WSH_{850,250}$, which would suppress TT development by hindering vertical alignment[1,48]. However, it is noteworthy that in both future periods (Fig. 3c, d), negative anomalies appear over parts of the central subtropics and the northern NATL (north of ~40°N). These regions of reduced WSH suggest localized environments more favorable for TT development, as lower values of $WSH_{850,250}$ allow TCs to maintain their vertical warm structure[20]. When considering the SSP5-8.5 scenario, the near-future period anomaly (Fig. 3e) presents weak negative anomalies across approximately the southern half of the domain, mostly between 20°N and 40°N, which suggests a slightly more favorable environment for TTs development and maintenance. Contrary to Vecchi and Soden[47], Michaelis and Lackmann[46], who use GCM simulations under the IPCC AR5 RCP8.5 emissions scenario, reported a reduction in WSH over the tropical Atlantic and increases across the northern part of the NATL, which coincides with the results shown in Fig. 3e, f. It should be noted that the statistically non-significant anomalies over large areas of the NATL for the near future period (Fig. 3e) indicate a limited impact during this period. Figure 3f shows stronger negative values of the max $WSH_{850,250}$ anomalies across a larger region, mostly between 10°N and 50°N, where the historical climatology maxima are observed (Fig. 3b), indicating the existence of environmental conditions more prone to TTs. It should be noted that there is a region that presents highly statistically significant positive anomaly values of the max $WSH_{850,250}$ over the Caribbean area for the far future period (Fig. 3f). Unlike SSP2-4.5, where the max $WSH_{850,250}$ strengthens across the entire tropical Atlantic (possibly as a response to positive ENSO events)[47], here the positive anomalies are more spatially confined, which could be due to the western Atlantic WSH response during positive ENSO phases[21]. This spatially heterogeneous pattern suggests that under extreme warming, ENSO influences can remain strong but act more regionally, with WSH intensification centered in the western tropical Atlantic and Caribbean, while the central and eastern tropical Atlantic experience reduced WSH. This dipole structure is consistent with the findings of Gray[42], who linked eastern Pacific warming with enhanced shear over the western Atlantic but not uniformly across the basin.

In Fig. 4a, differences between the minimum seasonal value (min) of the CI historical field of ERA5 and the multi-model CMIP6 composite show notable discrepancies primarily poleward of ~ 45°N, where positive differences are found, indicating stronger min CI values in ERA5 relative to CMIP6. In contrast, certain tropical regions and parts of northeastern Africa display negative differences, suggesting localized overestimation of min CI by the CMIP6 models. The central NATL exhibits no relevant differences between the datasets. This low discrepancy is particularly interesting, as the central basin constitutes our primary area of interest for TTs genesis and development[10]. In Fig. 4b, the min CI historical climatology can be seen, where the low values over the tropical Atlantic region indicate areas of weak atmospheric stability and favorable conditions for convection. Regions with min CI values below 22.5 °C (striped region; Fig. 4b) suggest environments conducive to deep convection and TT development[7], overlapping with low max $WSH_{850,250}$ regions (Fig. 3b).

For the near future period in both emission scenarios considered (Fig. 4c, e), negative min CI anomalies dominate most of the NATL basin, with reductions up to 4–8 °C. Figure 4d, f show the far future anomaly values, and it can be noted that they intensify across much of the NATL, with a reduction reaching up to −12 °C in some points of the northern domain. This substantial decrease highlights a more unstable atmosphere, favoring deeper convection and strengthening TTs, expanding the area below the 22.5 °C upper limit[10,15] for TTs development in both the near and the far future periods (Fig. 4c–f). The central-subtropical region presents statistically significant positive anomaly values when considering the SSP2-4.5 scenario (Fig. 4c, d), which is more intense for the far future period (Fig. 4d). This enhancement can be linked to the positive anomalies of max $WSH_{850,250}$ shown in Fig. 3c, d. The increase in max $WSH_{850,250}$ in this area may contribute to a greater atmospheric destabilization, which is reflected in the min CI field. Stronger WSH can modify the upper- and lower-level flow interactions, enhancing vertical gradients of momentum and potentially influencing the development or suppression of convective activity[7,10,22]. Therefore, this behavior suggests a dynamical linkage between WSH changes and the regional CI environment, reinforcing the physical consistency of the projected patterns. In Fig. 4e, f the positive anomalies in the central-subtropical region are not statistically significant, which is also in line with the appreciated in Fig. 3e, f, where the max $WSH_{850,250}$ anomalies are negative over the area, and can contribute to the stabilization of the atmosphere. Nevertheless, this different behavior in that specific region may be affected by other factors beyond the max $WSH_{850,250}$, such as the strong influence of local processes like the African Easterly Jet or the possible expansion of the Azores High over the area because of the ACC[49,50]. However, a deep analysis of these processes is beyond the scope of this study.

Climatological behavior of the Tropical Transition Favorability Index

After analyzing all the parameters that potentially influence tropical cyclogenesis via mid-latitude dynamics in the NATL, the tropical transition favorability index (TTFI) evolution throughout the XXI century is presented in Fig. 5. The ERA5 historical TTFI results display higher values over the central NATL when compared with the CMIP6 multi-models composite, particularly in its eastern-central sector, where positive differences of approximately 1.5 TTFI units are observed (Fig. 5a). This discrepancy is likely attributable to the higher SST values above mentioned (Fig. 1a) combined with the lower max $WSH_{850,250}$ in ERA5 (Fig. 3a), as SST and max $WSH_{850,250}$ represent the parameters with the largest deviations from the ERA5 dataset in that region. Figure 5b shows that the maximum values are reached over the central and western part of the NATL basin, indicating that this region is particularly conducive to TTs development during SON. The TTFI calculated from the real TT cases during the 1981 – 2010 period presents values ranging from an approximate minimum of 4 TTFI units at the outer edges of the TTs composite to an approximate maximum of 26 TTFI units near the center of the systems composite (Fig. S1a). Given this threshold, areas in Fig. 5b where the TTFI meets or exceeds 4 TTFI Units are marked with stripes, indicating regions where the minimum TTFI observed in real TT events is reached. This approach helps delineate zones that align with the most favorable TT environments.

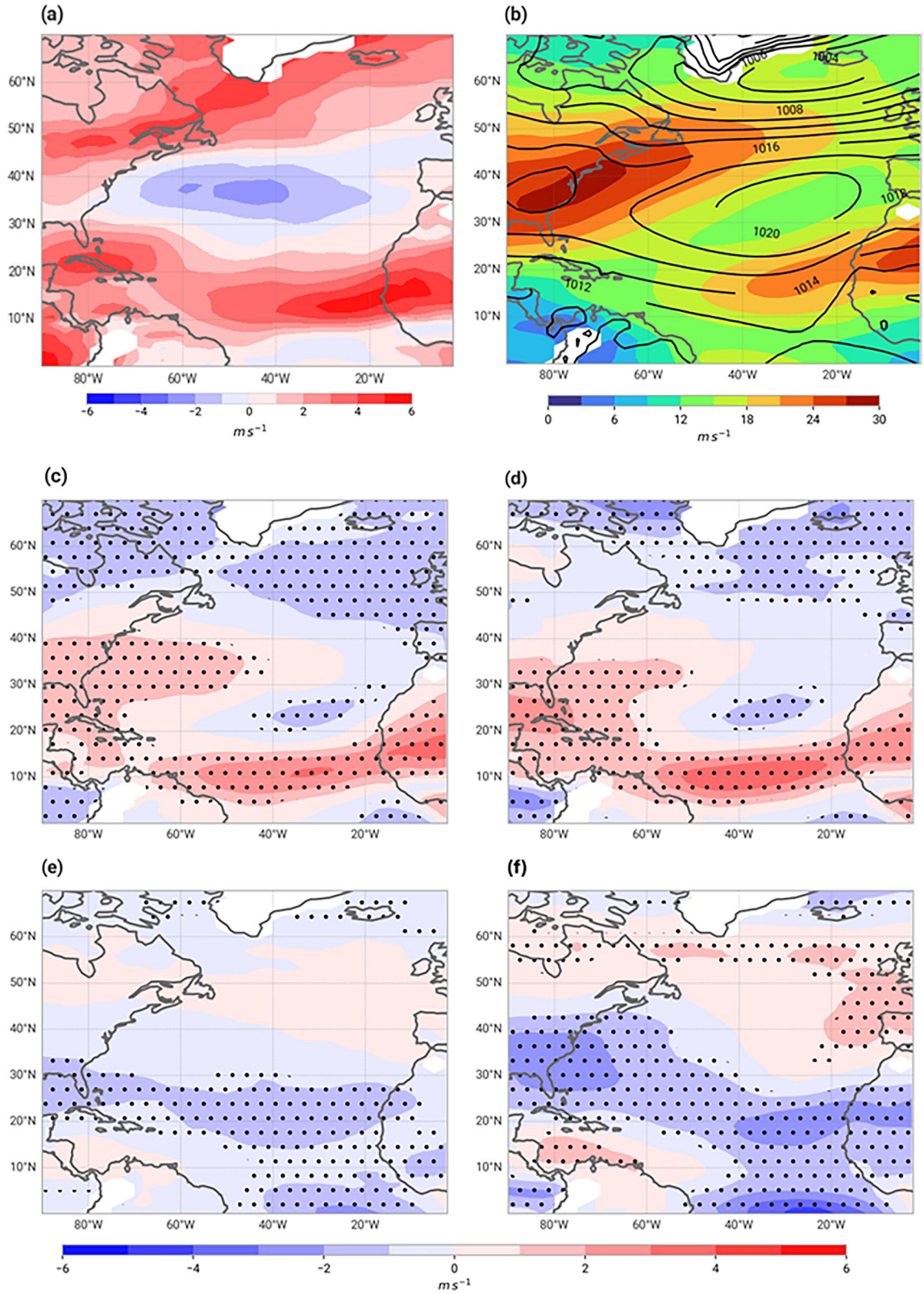

Fig. 3 | SON historical climatology, SSP2-4.5 and SSP5-8.5 projections of max $WSH_{850,250}$ in the NATL for the XXI century. a SON ERA5 historical climatology differences of max $WSH_{850,250}(ms^{-1})$ with respect to the multi-model CMIP6 composite. **b** SON historical climatology values from the multi-model CMIP6 composite of max $WSH_{850,250}(ms^{-1})$ and MSLP (hPa; black contours). SON anomaly values with respect to **b** of max $WSH_{850,250}(ms^{-1})$ for **c** near future period and **d** far future period considering the SSP2-4.5 scenario; with respect to **b** of max $WSH_{850,250}(ms^{-1})$ for **e** near future period and **f** far future period considering the SSP5-8.5 scenario. Black dots indicate statistically significant anomalies based on the Mann–Whitney U test ($\alpha = 0.05$).

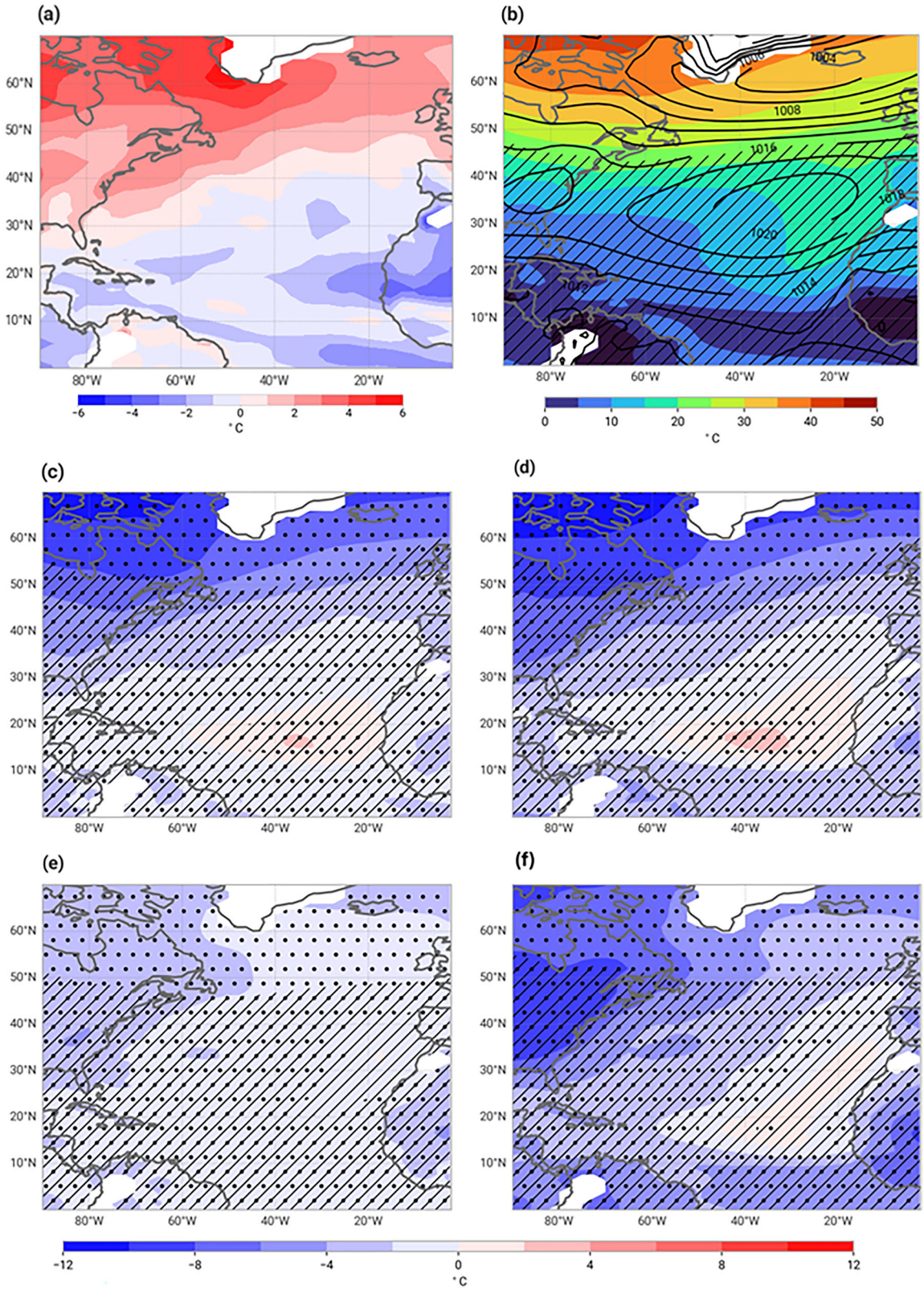

Fig. 4 | SON historical climatology, SSP2-4.5 and SSP5-8.5 projections of min CI in the NATL for the XXI century. a SON ERA5 historical climatology differences of min CI (°C) with respect to the multi-model CMIP6 composite. **b** SON historical climatology values from the multi-model CMIP6 composite of min CI (°C) and MSLP (hPa; black contours). SON anomaly values with respect to **b** of min CI (°C) for **c** near future period and **d** far future period considering the SSP2-4.5 scenario; with respect to **b** of min CI (°C) for **e** near future period and **f** far future period considering the SSP5-8.5 scenario. Black dots indicate statistically significant anomalies based on the Mann–Whitney U test ($\alpha = 0.05$). Stripped regions in (**b**) indicate where the min CI value is lower or equal to 22.5 °C; in (**c**–**f**) indicate where the min CI value is lower than or equal to 22.5 °C, adding the anomaly value to the **b** field.

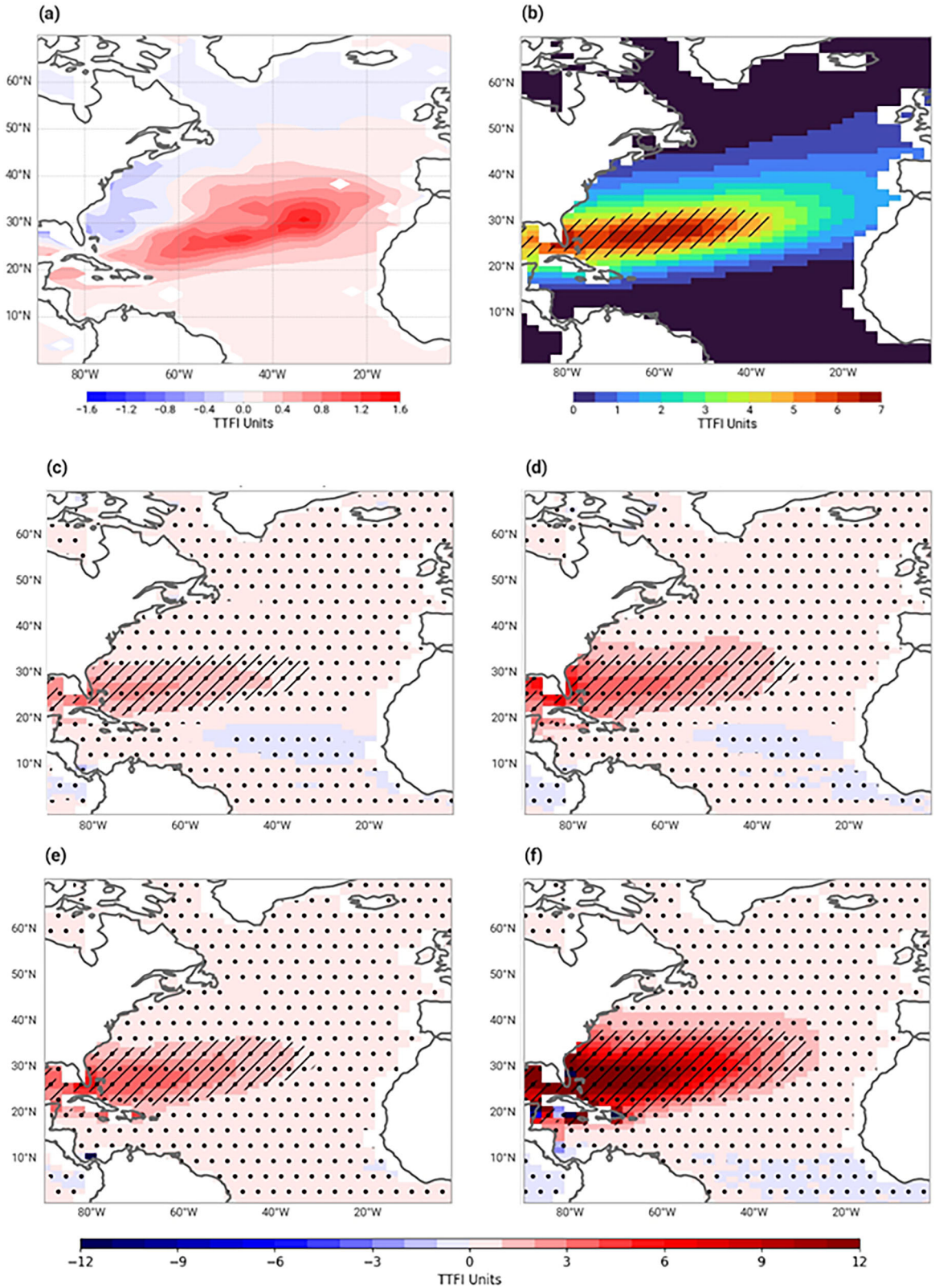

Fig. 5 | SON historical climatology, SSP2-4.5 and SSP5-8.5 projections of the TTFI in the NATL for the XXI century. a SON ERA5 historical climatology differences of the TTFI (TTFI Units) with respect to the multi-model CMIP6 composite. **b** SON historical climatology values from the multi-model CMIP6 composite of the TTFI (TTFI Units). SON anomaly values with respect to **b** for **c** near future period and **d** far future period considering the SSP2-4.5 scenario; with respect to **b** for **e** near future period and **f** far future period considering the SSP5-8.5 scenario. Black dots indicate statistically significant anomalies based on the Mann–Whitney U test ($\alpha = 0.05$). Striped regions in (**b**) indicate where the TTFI value is higher or equal to 4 TTFI Units; in (**c**–**f**) indicate where the TTFI value is higher or equal to 4 TTFI Units, adding the anomaly value to the **b** field.

Figure 5c, d reveal statistically significant positive anomaly values across the whole domain, with the most pronounced increases over the central-western NATL, especially in the far future period (Fig. 5d). This pattern is consistent with the results obtained from the analyzed parameters, all of which suggest an intensified tropicalization of the NATL. The higher TTFI values in the central-western NATL, appreciated in Fig. 5b, compared to the eastern part aligns with findings from Galarneau et al.[51] and Calvo-Sancho et al.[10], since they prove that the environmental conditions for TTs development have historically been less favorable in the eastern region. The observed NATL TT cases (from the HURDAT database) from 1981 to 2010 do not exactly coincide with the regions of maximum ERA5 historical TTFI values (Fig. S2a), which may be because the TTFI is a synoptic-scale index that does not account for mesoscale processes, which can locally influence TT cyclogenesis. Moreover, uncertainties associated with the representation of the Gulf Stream and the Labrador Current[52] may further contribute to these spatial differences. Nevertheless, the overall distribution of observed TTs development closely matches the areas of elevated values in the historical ERA5 TTFI climatology (Fig. S2a, black contours). This consistency indicates that the TTFI serves as a reliable metric for identifying regions favorable for TT development.

Under the influence of ACC, the TTFI undergoes a statistically significant increase, primarily in the central-western NATL, but also extending to northern and eastern parts of the NATL basin. It is important to note that the striped areas (TTFI ≥ 4 TTFI Units) expand substantially under the influence of the ACC in Fig. 5c-f. The increase in the spatial extent of regions exceeding the 4 TTFI Units threshold indicates a broader area becoming conducive to TTs development. This expansion is particularly pronounced in the far future period (Fig. 5d, f), where high TTFI values extend further north-eastward, being more pronounced for the SSP5-8.5 scenario (Fig. 5f). Such an intensification and expansion suggest that the eastern NATL, including its coastal regions, could experience an enhanced influence from TTs activity, potentially increasing the risk of TT-related impacts along the eastern NATL coast under both scenarios considered, but more specifically for the SSP5-8.5 one. As a result, the NATL becomes more conducive to TTs formation, especially toward the latter part of the XXI century. It should be noted that the anomaly values reach up to +12 TTFI Units in the far future period of the most extreme scenario (Fig. 5f), which nearly double the highest values obtained in the reference period (Fig. 5b). The TTFI behavior observed here is consistent with the patterns shown in Figs. S1b, c and S2b, c, which present the differences in TTs intensity and TTs density between the 1981–2023 and 1981–2010 periods, respectively. Figure S1b, c reveal an intensification of TTFI values for TTs that developed between 2010 and 2023, with increases of approximately 6 TTFI units in the core of the systems. Figures S2b, c indicate that TTs development in the NATL has notably increased over the central and western regions, with a clear eastward expansion, over the last decade. This intensification is consistent with the near-future TTFI projections shown in Fig. 5c, e, which also display statistically significant positive anomalies and an eastward extension of the regions exhibiting high TTFI values.

The spatial mean of the TTFI 95th percentile (P95) evolution for the historical, SSP2-4.5, and SSP5-8.5 scenarios is presented in Figure S3a, b, c, respectively. All three cases display statistically significant positive trends ($p \leq 0.05$), with the rate of increase being more pronounced in the SSP2-4.5 scenario compared to the historical period, and even stronger under SSP5-8.5. A progressive enhancement of the trend is observed with increasing TTFI percentiles, suggesting that higher values experience stronger growth rates (not shown). The results indicate that extreme TTFI values are increasing, which is consistent with the trend shown in Fig. 5c–f, suggesting that ACC highly influences it. The higher slopes observed under both future scenarios, particularly SSP5-8.5, further support the conclusion that stronger forcing conditions are associated with a more rapid increase of extreme TTFI magnitudes. These results suggest that both the frequency of real TTs and the intensity of their TTFI value in the NATL have increased in recent decades, following a trend that is projected to continue under future climate scenarios.

CMIP6 inter-model consistency analysis

In addition to the mean parameters' patterns and behavior described above, an analysis of the CMIP6 inter-model consistency is carried out. The examination of the signal-to-noise ratio (S/N), defined as the ensemble mean divided by the inter-model standard deviation, offers key insights into inter-model consistency. For SST, low S/N values in the northwestern NATL indicate strong uncertainty and modeling challenges that can be related to the interaction between the Gulf Stream and the Labrador Current[52]. However, S/N values exceeding unity across most of the basin reflect high agreement among models in the historical and both future anomalies' projections under SSP2-4.5 and SSP5-8.5 (Fig. S4). Similar consistency is observed for the TCW (Fig. S5) and the max $WSH_{850,250}$ (Fig. S6), where S/N > 1 suggests reliable anomalies' projections, despite some localized regions with higher uncertainty for the max $WSH_{850,250}$. The min CI (Fig. S7) shows larger inter-model discrepancies since S/N < 1 is observed in the area of interest, whose reasons are interesting to analyze in future research. Because of the lower min CI S/N values, the TTFI S/N (Fig. S8) presents inter-model inconsistency in the southern half of the studied domain. Nevertheless, when the S/N analysis is applied to the projected fields themselves rather than to their anomalies (Fig. S10), a much higher degree of consistency among models becomes evident. This suggests that, despite differences in the magnitude of anomalies relative to the historical climatology, the models generally converge on the large-scale spatial structure of TTFI under future climate conditions. Such an agreement reinforces confidence in the robustness of the underlying climatological patterns, even though the amplitude of projected changes remains uncertain. Overall, the probability density function (PDF; Fig. S9) analyses confirm that individual CMIP6 models and the multi-model ensemble display statistically consistent distributions (mean p-values > 0.05) for all parameters considered. This coherence supports the robustness of the ensemble in representing both historical and projected conditions across the North Atlantic. For a more detailed discussion, consult the supplementary material.

Discussion

The impact of ACC on tropical cyclogenesis has become a pressing concern due to the destructive nature of these events[1,2]. Europe, a region unaccustomed to such phenomena, has already experienced their adverse effects[10,33]. While projections suggest that these systems will continue to affect areas traditionally spared from their influence[17,25], large uncertainty remains regarding the extent and timing of these changes[29,53], highlighting the need for further research and refined modeling efforts. For this reason, this study researches the climatology of NATL environments favorable for TTs, focusing on the influence of ACC during the autumn months, when TTs are most frequent over the area of interest. Key parameters related to TTs development are analyzed across three time periods: historical (1981–2010), near future (2021–2050), and far future (2071–2100). The analysis uses composite data from ten CMIP6 climate models under historical, SSP2-4.5, and SSP5-8.5 scenarios.

The results highlight the critical role of rising SST in the intensification and poleward migration of TCs through the TT mechanism in the NATL basin. Historical SST data reveal temperatures above 25.5 °C dominate tropical and subtropical regions, a threshold crucial for TC development[18]. Projected SST anomalies for the near and far future indicate widespread warming, with late-century scenarios showing a stronger SST increase over the whole domain of study. These trends are accompanied by statistically significant increases in atmospheric moisture. Additionally, the wind shear and the atmospheric stability are analyzed, as both are key dynamic factors that influence TT's development. High wind shear values weaken cyclones by tilting their vertical structure, while low to moderate values support cyclogenesis, particularly during interactions with midlatitude systems[8,15]. Future projections of vertical wind shear reveal contrasting responses between emission scenarios. Under the moderate SSP2-4.5 pathway, persistently positive anomalies are projected across the tropical and central-western Atlantic, intensifying toward the late century, consistent with

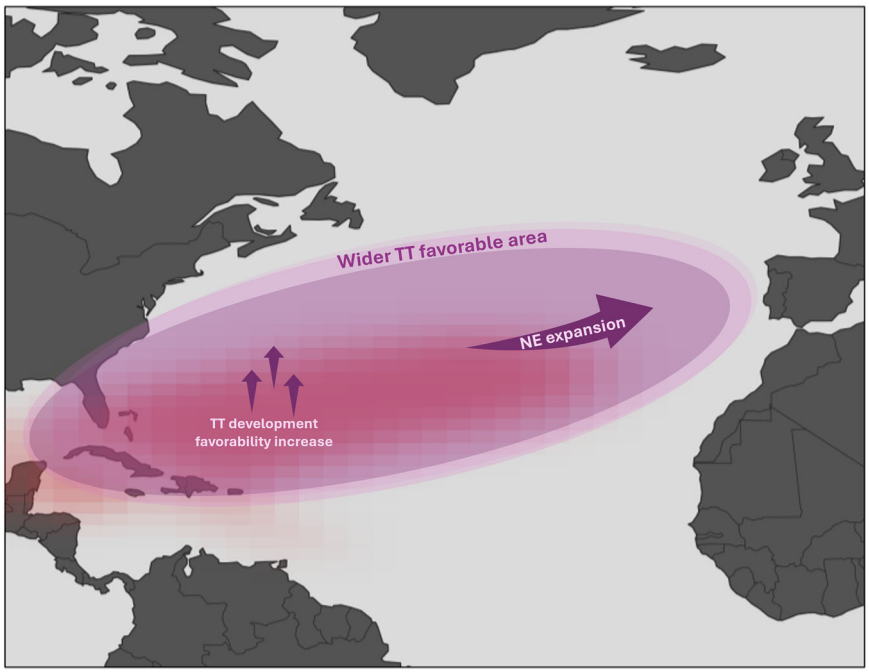

Fig. 6 | Scheme of the projected evolution of the NATL TT favorable environment during SON in the XXI century. Scheme of the projected evolution of the NATL environment favorable for TTs during SON in the XXI century under ACC. Red shading indicates the historical favorable region, and light purple shading marks the projected northeastward expansion. Arrows depict the enhancement of favorable conditions and the direction of expansion.

Vecchi and Soden[47], who reported similar increases under the A1B scenario. Such strengthening would likely suppress tropical TT development by disrupting vertical storm alignment[1,48]. In contrast, the high-emission SSP5-8.5 scenario shows a near-future period with limited change, followed by widespread and statistically significant negative WSH anomalies between 10°N and 50°N in the far future, suggesting a more favorable environment for TT occurrence[20,46]. While SSP2-4.5 produces a relatively uniform strengthening of WSH across the tropical Atlantic, SSP5-8.5 displays a dipole structure with enhanced shear over the Caribbean and reduced shear in the central and eastern basin, possibly linked to ENSO-related variability[21,42]. Low values of atmospheric stability promote convection[15], and future projections reveal statistically significant atmospheric stability reductions over most of the domain. This, combined with warming SST, higher moisture content, and lower wind shear, indicates a future environment more conducive to TTs in a warming climate under the two emission scenarios considered.

A novel aspect of this study is the projected evolution throughout the current century of a newly developed index, the TTFI, which is related to environments favorable for TTs in the midlatitudes. This approach enables a more precise understanding of the intricate dynamics and thermodynamics aspects that drive tropical cyclogenesis via mid-latitude dynamics in the NATL, as the index allows to determine whether enhancing thermodynamic parameters behavior may counterbalance or amplify the influence of hindering dynamic parameters. The analysis reveals a statistically significant increase in the TTFI across the NATL basin, particularly in the central-western region, indicating a growing tendency toward tropicalization. Notably, under both the SSP2-4.5 and the SSP5-8.5 scenarios, areas exceeding the 4 TTFI unit threshold (observed minimum for TT formation in the NATL) expand considerably (more pronounced for the SSP5-8.5 scenario), suggesting a broader region becoming conducive to TTs development. By the late part of the century, this expansion extends northeastward, implying greater TTs activity and potential impacts along the eastern NATL coast. These projected changes are summarized schematically in Fig. 6, which provides a conceptual overview of the historical TT favorable region (red area) that intensifies and expands northeastwardly (light purple shading) during the XXI century. The study also reveals a large increase in the spatial mean of the TTFI P95 evolution, a trend that is more pronounced under the high-emission SSP5-8.5 scenario. Moreover, this projection is consistent with an observed increase in real TTs density in the NATL and their TTFI values over the last decade. It is noteworthy to point out that the region of maximum TTFI is located around 30°N and generally equatorward of the midlatitude jet, implying that many TT systems forming within this band may eventually interact with the baroclinic zone and undergo extratropical transition. During or after this process, some systems can reintensify as they couple with upper-level troughs and gain baroclinic energy[34,54–56]. This interaction often results in hybrid or post-tropical cyclones capable of producing strong winds and heavy precipitation across mid-latitude regions, including Western Europe[4]. These processes represent additional determinants of risk that should be acknowledged when assessing future TT-related hazards.

It is important to continue monitoring and improving the modeling of TTs development in the NATL, particularly under high-emission scenarios, since TCs forming via the TT pathway may become more frequent and capable of impacting higher latitudes according to these study results. An increased occurrence of TTs may have important socio-economic implications for the NATL coastal regions. However, these findings should be interpreted with caution due to uncertainties inherent in the TTFI's parameters, which can influence the robustness of the projections. In some cases, the magnitude of the projected future changes is comparable to the existing CMIP6 models biases with respect to ERA5. This underscores the need for further research to constrain these uncertainties while acknowledging the serious implications for future economic losses, infrastructure damage, and human casualties.

Methods

The main purpose of this study is to establish a forecasted relationship between the ACC and the NATL environment tendency throughout the XXI century of some specific parameters related to TTs (Table 1). The analysis is carried out for SON, as most cyclones affecting Europe that originate from TTs occur during this season[10]. Therefore, the domain studied is 00°N - 70°N, 90°W - 00°E since it covers the region of interest, and the period analyzed spans from 1980 to 2100. The SSP2-4.5 and SSP5-8.5 scenarios[57] are used to compute the difference between the historical climatology (1981–2010) and the climatology of two future periods sufficiently spaced in time so that they represent different situations: the near future (2021–2050) and the far future (2071–2100) periods. On the one hand, the SSP2-4.5 scenario represents an intermediate greenhouse gases emissions pathway, often referred to as a *"middle-of-the-road"* scenario[36]. On the other

hand, the SSP5-8.5 scenario is the most extreme one, which offers a robust basis for assessing potential climate impacts and enables researchers to investigate the upper limits of environmental changes, in agreement with Guan et al.[58] and Yaddanapudi et al.[59] Therefore, considering these two scenarios is valuable for capturing both the moderate and the far-reaching consequences of future NATL environmental changes in the context of tropical cyclogenesis via mid-latitude dynamics.

Parameters

The parameters analyzed in Montoro-Mendoza et al.[11] are studied here using a different methodology so that ten climate models from the CMIP6 repository can be considered instead of just one. Montoro-Mendoza et al.[11] employ an adapted version of the EC-Earth3 model due to the requirement of some specific variables for the methodology used there, like the θ_{DT}, which enables more precise CI calculations. However, the current study makes an approximation of those variables through some calculations (specified hereafter in this section) to use a larger number of climate models. In order to provide an adequate baseline for comparison, the historical climatology of all analyzed parameters is computed using monthly data for the SON season from the ERA5 reanalysis dataset[60]. This step is essential for evaluating the consistency and biases of the CMIP6 multi-model composites (Table 2) against observational data. This way, it is possible to assess the models' performance in reproducing historical climate conditions, which provides valuable insights into potential systematic biases, thereby contributing to a more comprehensive understanding of the analyzed parameters.

Seasonal anomalies for SON in the near and far future, relative to the historical SON baseline, are calculated, and their statistical significance is evaluated using the Mann-Whitney U test[61] with a significance level of $\alpha = 0.05$. Table 1 outlines the parameters employed in this analysis. Regardless of the origin, TCs development, maintenance, and intensity are highly influenced by the SST, TCW, and WSH (Eq. 1), according to several previous studies such as Riehl[45], DeMaria et al.[43] and Calvo-Sancho et al.[10]. Additionally, the CI (Eq. 2) is particularly relevant for studying TCs whose origin is a TT[10,15,16].

Table 1 | Parameters analyzed

Parameter	*Acronym*	*Units*
Sea Surface Temperature	SST	°C
Total Column Water	TCW	mm
Vertical Wind Shear (800–250 hPa)	$WSH_{850,250}$	ms^{-1}
Coupling Index	CI	°C
Tropical Transition Favorability Index	TTFI	$10^{-3} kgs^2 mm^{-2} K^{-1}$ (TTFI Units)

To assess ensemble agreement, the Probability Density Function (PDF) is calculated for each parameter and scenario used. The PDF of each individual climate model is compared against the corresponding ensemble mean PDF and, for the historical period, also against the ERA5 reanalysis PDF, using the Mann–Whitney U test[61]. The arithmetic mean of the resulting p-values is computed for each variable-scenario combination. These mean *p*-values serve as measures of ensemble similarity: values greater than 0.05 indicate that the models are statistically consistent, and that both the ensemble mean and the ERA5 dataset (for the historical period) provide robust representations. Additionally, to quantify the degree of inter-model consensus and to identify the regions where the projected changes can be interpreted with higher confidence, the signal-to-noise ratio (S/N) is computed for each parameter, scenario, and period considered in the TTFI calculation (Eq. 3). Firstly, the historical S/N is obtained by calculating the standard deviation (std) of each parameter's historical field across the ten CMIP6 models. The multi-model CMIP6 composite of that parameter is then divided by the corresponding std. When the resulting S/N value exceeds unity, it indicates a robust agreement among the historical climatology of the selected CMIP6 models. In the second step, the same procedure is applied to the anomaly fields. Specifically, the anomaly pattern for each scenario-period-parameter combination is computed and divided by the std derived from the ten CMIP6 models. Similarly, when the S/N value is greater than unity, the anomalies' projection is considered consistent among models.

This study employs monthly mean data directly downloaded from the CMIP6 repository for all parameters. The composite data (by computing the arithmetic average) from the ten models selected (Table 2) is considered for each of the parameters analyzed to obtain a consistent representation of the environment trends. Furthermore, the MetPy (*metpy.calc*) Python package[62] is used to derive additional variables, such as the θ_E and the potential temperature (θ), both of which are essential for computing the CI (Eq. 2).

The WSH, considering the vertical levels 250 hPa and 850 hPa, is computed following Eq. 1.

$$WSH_{850,250} = \sqrt{(u_{250} - u_{850})^2 + (v_{250} - v_{850})^2} \quad (1)$$

where u_{250}, u_{850} and v_{250}, v_{850} are the wind components at 250 hPa and 850 hPa, respectively.

The CI expression is specified in Eq. 3 (Bosart and Lackman, 1995).

$$CI = \theta_{DT} - \theta_{E,850} \quad (2)$$

where $\theta_{E,850}$ is the equivalent potential temperature at 850 hPa and θ_{DT} is the potential temperature at the dynamic tropopause, approximated by averaging the potential temperature at 200 hPa and 300 hPa.

Table 2 | CMIP6 models selected

Climatic model	Horizontal resolution	Vertical resolution	Ensemble member	Reference
IPSL-CM6A-LR	1.3 × 2.5°	79 levels	r1i1p1f1	Boucher et al.[67]
INM-CM4-8	1.5° x 2°	21 levels	r1i1p1f1	Volodin et al.[68]
MIROC6	1.4° x 1.4°	81 levels	r1i1p1f1	Tatebe et al.[69]
HadGEM3-GC31-MM	0.83° x 0.56°	85 levels	r1i1p1f3	Roberts et al.[70]
EC-Earth3	0.7° x 0.7°	91 levels	r5i1p1f1	Döscher et al.[71]
MPI-ESM1-2-HR	0.93° x 0.93°	95 levels	r1i1p1f1	Gutjahr et al.[72]
CESM2-WACCM	1.3° x 0.9°	70 levels	r1i1p1f1	Danabasoglu[73]
MRI-ESM2-0	1.12° x 1.13°	80 levels	r1i1p1f1	Yukimoto et al.[74]
NorESM2-MM	0.94° x 1.25°	32 levels	r2i1p1f1	Seland et al.[75]
GISS-E2-1-G	2° x 2.5°	40 levels	r2i1p3f1	Kelley et al.[76]

It should be noted that mean values of the $WSH_{850,250}$ and the CI smooth the result and do not adequately contribute to the understanding of the effect these parameters behavior can have on tropical cyclogenesis, which is in line with Montoro-Mendoza et al.[11] For this reason, the extreme values of these parameters are emphasized in this study by computing the max $WSH_{850,250}$ and min CI for each year, since high $WSH_{850,250}$ impacts the structural dynamics of TCs and reduced CI fosters atmospheric instability and supports robust convection, enabling a smoother and more effective TT process[10,16].

Tropical Transition Favorability Index

A comprehensive evaluation of the combined effect of all parameters is essential to determine whether certain factors may counterbalance or amplify the influence of others. This approach allows for a more accurate assessment of the complex interactions that govern tropical cyclogenesis via mid-latitude dynamics in the NATL basin. Specifically, it is necessary to research whether opposing forces might mitigate the expected impacts of favorable conditions, thereby influencing the extent and likelihood of tropicalization of the NATL. Therefore, the TTFI is defined here (Eq. 3) to jointly assess the effectiveness of the parameters that promote environments conducive to TTs in the NATL basin:

$$TTFI = \frac{TCW \cdot SST}{\max\left(WSH_{850,250}\right) \cdot \min(CI)} \cdot \mathrm{M} \quad (3)$$

where M represents a Gaussian probability density function that provides latitudinal weights (Fig. S11) fixed to enhance the spatial accuracy of the index, emphasizing regions historically prone to NATL TTs. This weighting function refines the spatial distribution by accounting for the preferred latitudinal zones of TT occurrence. Specifically, the mean ($\mu = 30.67°$) and standard deviation ($\sigma = 5.33°$) of M are calculated using the latitudinal positions of cyclone tracks that transitioned into TCs within the NATL between 1981 and 2010, following the TTs identification methodology of Calvo-Sancho et al.[10], excluding latitudes below 20°N to disregard the influence of tropical waves[63]. Anchoring the M parameters to real TT cases ensures that the TTFI accurately highlights the NATL extratropical regions susceptible to TTs development while avoiding overemphasis on tropical zones where conventional TC formation dominates[6]. Additionally, to assess the index response to potential future northern shifts in TCs occurrence, M has been set to unity for areas located north of the calculated μ. This modification accounts for projections from other studies[14,28], suggesting a potential northward migration of TCs in response to ACC, which ensures that the TTFI remains a useful tool for evaluating future tropical cyclogenesis patterns via mid-latitude dynamics. This approach provides a more precise depiction of TT-prone regions in the NATL. Consequently, the index serves as a valuable tool for assessing the evolving risk of TTs development under changing climate scenarios.

The TTFI is designed to capture the environmental conditions favorable for TTs development by integrating the key parameters (Table 1) that influence the process. The formulation considers the thermodynamic and dynamic drivers of TTs, offering a comprehensive evaluation of the contributing parameters. Namely, the TTFI is the ratio of thermodynamic factors that enhance TTs to dynamic ones, which generally hinder TTs development. It is important to note, however, that dynamic factors such as moderate WSH may initially aid the organization of the precursor baroclinic disturbance before becoming unfavorable to further tropical intensification[7,10,20]. On the one hand, high values of SST and TCW enhance the TTs development by providing the necessary heat and moisture. Consequently, both parameters are placed in the numerator of the TTFI equation, promoting a rise in the index when favorable thermodynamic conditions prevail. On the other hand, low values of max $WSH_{850,250}$ and min CI facilitate TTs development[10,15]. Thus, these parameters serve as the denominator in Equation 4, ensuring that unfavorable dynamic conditions lead to a decrease in the TTFI. To establish a baseline, the TTFI historical climatology for SON is calculated using ERA5[60] monthly data, essential for assessing the selected CMIP6 models (Table 2) composite biases and consistency against observations.

To examine regions of real NATL TTs development and assess their correspondence with high TTFI values, the development map of real NATL TT cases is compared against the historical TTFI ERA5 climatology (Fig. S2a). The methodology described in Calvo-Sancho et al.[10] is used to identify the real NATL TT cases, covering the 1981–2010 period across the entire NATL basin, excluding latitudes below 20°N to disregard the influence of tropical waves[63], as above indicated. These comparisons serve to validate the effectiveness of the TTFI in capturing the environmental conditions conducive to TTs development and provide a basis for evaluating its reliability in future climate scenarios. Furthermore, to assess the TTFI value in real TT cases, the composite of the parameters listed in Table 1 for a set of observed TT events in the NATL is obtained, downloading the necessary data from the ERA5 global reanalysis dataset[60]. The TTFI is then calculated following Eq. 4 (Fig. S1a). By following this approach, the TTFI climatological values can be directly compared to the composite of the TTFI obtained from the real NATL TTs. Additionally, to characterize recent trends, both the TTFI intensity and the development density of real TTs (HURDAT database) are computed for the 1981-2023 period (Fig. S1b, S2b, respectively) and compared with the 1981-2010 baseline, allowing to establish differences between the historical and recent decades (Fig. S1c, S2c, respectively).

Finally, several TTFI percentiles are calculated (not shown) to examine how the TTFI behaves across different intensity thresholds, covering from 1981 to 2100. Among them, the spatial mean of the TTFI P95 evolution from the multi-model CMIP6 composite is presented for the historical, SSP2-4.5, and SSP5-8.5 scenarios (Fig. S3a–c), since higher percentiles exhibit a more pronounced increase over time, providing a clearer representation of the intensification of extreme TTFI values over time under future climate conditions.

CMIP6 models used

For this study, ten CMIP6 models are selected (Table 2), and each of them contributes specific strengths. This broader multi-model approach is particularly relevant, according to studies such as Camargo et al.[40], who highlight that the climatology of TC-like storms in CMIP6 has improved compared with CMIP5, mainly due to increased horizontal resolution across the ensemble. However, important model-dependent factors still introduce considerable variability and biases in TC representation[40]. It is important to highlight that CMIP6 models are insufficient to examine events and, therefore, analysis should be restricted to environmental fields. Therefore, by expanding the analysis beyond a single model, the present study aims to capture this inter-model consistency and provide a more statistically robust perspective, even though the approximation of certain variables may result in higher uncertainty, like the CI (Fig. S7).

TCs require ocean-atmosphere coupled models to accurately simulate their intensity, development mechanisms, and interactions with large-scale circulation[19]. The selected coupled models operate at the global scale with different horizontal and vertical resolutions (Table 2), integrating atmospheric, oceanic, land, and sea ice components. Their inclusion is supported by strong results obtained in previous studies focused on the NATL[64–66], as well as the availability of the necessary variables in the CMIP6 repository (Table 1). IPSL-CM6A-LR offers refined aerosol-cloud interactions and carbon cycle feedbacks, enhancing its simulation of SST, AMOC, and Arctic Sea ice compared to its predecessors[67]. INM-CM4-8, although simpler in structure and with lower vertical resolution than some other CMIP6 models, has proven capable of capturing large-scale ocean-atmosphere dynamics that are essential for TC activity projections[68]. MIROC6 incorporates improvements in cloud processes, radiation, and ocean circulation, particularly enhancing the simulation of tropical and midlatitude dynamics[65,69]. HadGEM3-GC31-MM stands out for reducing surface biases in SST and precipitation over the Atlantic, improving TC representation[64,65,70]. EC-Earth3 integrates updated physics and coupling, improving variability and feedback simulations across the atmosphere-ocean-sea ice system[71]. Moreover, it successfully captures the behavior of northeast Atlantic surface

winds under climate change scenarios, a critical factor influencing TCs development[66]. MPI-ESM1-2-HR strengthens the representation of ENSO, AMOC, and regional climate variability[64,72]. CESM2-WACCM extends the standard CESM framework with an interactive stratosphere and mesosphere, enabling the assessment of stratosphere-troposphere coupling and its implications for TC pathways[73]. MRI-ESM2-0 offers detailed ocean-atmosphere coupling and has demonstrated skill in reproducing SST variability relevant to the western Pacific and NATL[74]. NorESM2-MM shares physical components with CESM but includes unique treatments of aerosols and ocean biogeochemistry, making it valuable for studying the influence of atmospheric composition on TC-relevant processes[75]. Finally, GISS-E2-1-G features updated atmospheric physics and ocean coupling, improving energy balance representation and enabling robust simulations of TC-related climatology at coarse resolution[76]. These ten models provide a complementary ensemble of CMIP6 coupled simulations, whose combined use offers a robust framework for assessing future changes in NATL tropical cyclogenesis under different forcing scenarios.

Data availability

The selected CMIP6 climate models data can be obtained from the Earth System Grid Federation (ESGF) dataset, which is available online at: https://aims2.llnl.gov/search. Observational data from the ERA5 reanalysis can be obtained from the Copernicus Climate Data Store, available online at: https://cds.climate.copernicus.eu/datasets. The code used for the calculation of the TTFI in the NATL basin covering from 1981 to 2100, based on several CMIP6 models and ERA5, and the composite of the TTFI for a set of observed TT events in the NATL for the period 1981 – 2010, based on ERA5, are available from the corresponding author upon reasonable request.

Received: 15 May 2025; Accepted: 29 December 2025;
Published online: 09 January 2026

References

1. Pielke, R. A. & Landsea, C. W. Normalized Hurricane Damages in the United States: 1925–95. *Weather Forecast* **13**, 621–631 (1998).
2. Emanuel, K. Increasing destructiveness of tropical cyclones over the past 30 years. *Nature* **436**, 686–688 (2005).
3. Peduzzi, P. et al. Global trends in tropical cyclone risk. *Nat. Clim. Change* **2**, 289–294 (2012).
4. Haarsma, R. J. et al. More hurricanes to hit western Europe due to global warming. *Geophys. Res. Lett.* **40**, 1783–1788 (2013).
5. Baker, A. J., Hodges, K. I., Schiemann, R. K. H. & Vidale, P. L. Historical variability and lifecycles of north atlantic midlatitude cyclones originating in the tropics. *J. Geophys. Res. Atmos.* **126**, e2020JD033924 (2021).
6. González-Alemán, J. J., Valero, F., Martín-León, F. & Evans, J. L. Classification and Synoptic Analysis of Subtropical Cyclones within the Northeastern Atlantic Ocean. *J. Clim.* **28**, 3331–3352 (2015).
7. McTaggart-Cowan, R., Galarneau, T. J., Bosart, L. F., Moore, R. W. & Martius, O. A Global Climatology of Baroclinically Influenced Tropical Cyclogenesis. *Mon. Weather Rev.* **141**, 1963–1989 (2013).
8. Davis, C. A. & Bosart, L. F. Baroclinically Induced Tropical Cyclogenesis. *Mon. Weather Rev.* **131**, 2730–2747 (2003).
9. Quitián-Hernández, L., Martín, M. L., González-Alemán, J. J., Santos-Muñoz, D. & Valero, F. Identification of a subtropical cyclone in the proximity of the Canary Islands and its analysis by numerical modeling. *Atmos. Res.* **178–179**, 125–137 (2016).
10. Calvo-Sancho, C. et al. An environmental synoptic analysis of tropical transitions in the central and Eastern North Atlantic. *Atmos. Res.* **278**, 106353 (2022).
11. Montoro-Mendoza, A. et al. Environments conductive to tropical transitions in the North Atlantic: Anthropogenic climate change influence study. *Atmos. Res.* **310**, 107609 (2024).
12. Hulme, A. L. & Martin, J. E. Synoptic- and Frontal-Scale Influences on Tropical Transition Events in the Atlantic Basin. Part II: Tropical Transition of Hurricane Karen. *Mon. Weather Rev.* **137**, 3626–3650 (2009).
13. Cammas, J.-P., Keyser, D., Lackmann, G. M., & Molinari, J. Diabatic redistribution of potential vorticity accompanying the development of an outflow jet within a strong extratropical cyclone. In *Preprints, International Symposium on the Life Cycles of Extratropical Cyclones, Vol. II* 403–409 (Geophysical Institute, University of Bergen, Bergen, Norway, 1994).
14. Knutson, T. et al. Tropical Cyclones and Climate Change Assessment: Part I: Detection and Attribution. *Bull. Am. Meteorol. Soc.* **100**, 1987–2007 (2019).
15. McTaggart-Cowan, R., Davies, E. L., Fairman, J. G., Galarneau, T. J. & Schultz, D. M. Revisiting the 26.5 °C Sea Surface Temperature Threshold for Tropical Cyclone Development. *Bull. Am. Meteorol. Soc.* **96**, 1929–1943 (2015).
16. Kang, N.-Y. & Elsner, J. B. Trade-off between intensity and frequency of global tropical cyclones. *Nat. Clim. Change* **5**, 661–664 (2015).
17. Pérez-Alarcón, A., Fernández-Alvarez, J. C., Sorí, R., Nieto, R. & Gimeno, L. The Combined Effects of SST and the North Atlantic Subtropical High-Pressure System on the Atlantic Basin Tropical Cyclone Interannual Variability. *Atmosphere* **12**, 329 (2021).
18. Dare, R. A. & McBride, J. L. The Threshold Sea Surface Temperature Condition for Tropical Cyclogenesis. *J. Clim.* **24**, 4570–4576 (2011).
19. Hendricks, E. A., Peng, M. S., Fu, B. & Li, T. Quantifying Environmental Control on Tropical Cyclone Intensity Change. *Mon. Weather Rev.* **138**, 3243–3271 (2010).
20. Knutson, T. et al. Tropical Cyclones and Climate Change Assessment: Part II: Projected Response to Anthropogenic Warming. *Bull. Am. Meteorol. Soc.* **101**, E303–E322 (2020).
21. Aiyyer, A. R. & Thorncroft, C. Climatology of Vertical Wind Shear over the Tropical Atlantic. *J. Clim.* **19**, 2969–2983 (2006).
22. Rios-Berrios, R. et al. A Review of the Interactions between Tropical Cyclones and Environmental Vertical Wind Shear. *J. Atmos. Sci.* **81**, 713–741 (2024).
23. Kossin, J. P., Emanuel, K. A. & Vecchi, G. A. The poleward migration of the location of tropical cyclone maximum intensity. *Nature* **509**, 349–352 (2014).
24. Duan, H., Chen, D. & Lie, J. The Impact of Global Warming on Hurricane Intensity. *IOP Conf. Ser. Earth Environ. Sci.* **199**, 022045 (2018).
25. Walsh, K. J. E. et al. Tropical cyclones and climate change. *Trop. Cyclone Res. Rev.* **8**, 240–250 (2019).
26. Murakami, H. et al. Detected climatic change in global distribution of tropical cyclones. *Proc. Natl. Acad. Sci.* **117**, 10706–10714 (2020).
27. Wu, L., Zhao, H., Wang, C., Cao, J. & Liang, J. Understanding of the Effect of Climate Change on Tropical Cyclone Intensity: A Review. *Adv. Atmos. Sci.* **39**, 205–221 (2022).
28. Studholme, J., Fedorov, A. V., Gulev, S. K., Emanuel, K. & Hodges, K. Poleward expansion of tropical cyclone latitudes in warming climates. *Nat. Geosci.* **15**, 14–28 (2022).
29. Cao, X. et al. The southward shift of hurricane genesis over the northern Atlantic Ocean. *Npj Clim. Atmos. Sci.* **8**, 37 (2025).
30. Holland, G. & Bruyère, C. L. Recent intense hurricane response to global climate change. *Clim. Dyn.* **42**, 617–627 (2014).
31. Vecchi, G. A. & Knutson, T. R. On Estimates of Historical North Atlantic Tropical Cyclone Activity*. *J. Clim.* **21**, 3580–3600 (2008).
32. Vecchi, G. A. & Knutson, T. R. Estimating Annual Numbers of Atlantic Hurricanes Missing from the HURDAT Database (1878–1965) Using Ship Track Density. *J. Clim.* **24**, 1736–1746 (2011).
33. Guishard, M. P., Evans, J. L. & Hart, R. E. Atlantic Subtropical Storms. Part II: Climatology. *J. Clim.* **22**, 3574–3594 (2009).
34. Ribberink, M., De Vries, H., Bloemendaal, N., Baatsen, M. & Van Meijgaard, E. Tropical cyclone intensification and extratropical transition under alternate climate conditions: a case study of

Hurricane Ophelia (2017). Preprint at https://doi.org/10.5194/egusphere-2025-218 (2025).
35. Fox-Kemper, B. Ocean, Cryosphere and Sea Level Change. In vol. 2021. U13B-09 (2021).
36. Pörtner, H. O. et al. Summary for Policymakers. In *Climate Change 2022: Impacts, Adaptation and Vulnerability* (Intergovernmental Panel on Climate Change, Geneva, Switzerland, 2022).
37. Bentley, A. M., Bosart, L. F. & Keyser, D. Upper-Tropospheric Precursors to the Formation of Subtropical Cyclones that Undergo Tropical Transition in the North Atlantic Basin. *Mon. Weather Rev.* **145**, 503–520 (2017).
38. Eyring, V. et al. Overview of the Coupled Model Intercomparison Project Phase 6 (CMIP6) experimental design and organization. *Geosci. Model Dev.* **9**, 1937–1958 (2016).
39. Tebaldi, C. & O'Neill, B. C. Climate scenarios and their relevance and implications for impact studies. In *Climate Extremes and Their Implications for Impact and Risk Assessment* 11–29 (Elsevier, https://doi.org/10.1016/B978-0-12-814895-2.00002-1 2020).
40. Camargo, S. J. et al. Tropical Cyclones and Associated Environmental Fields in CMIP6 Models. *J. Clim.* **38**, 3877–3902 (2025).
41. Garcia-Soto, C. et al. An Overview of Ocean Climate Change Indicators: Sea Surface Temperature, Ocean Heat Content, Ocean pH, Dissolved Oxygen Concentration, Arctic Sea Ice Extent, Thickness and Volume, Sea Level and Strength of the AMOC (Atlantic Meridional Overturning Circulation). *Front. Mar. Sci.* **8**, 642372 (2021).
42. Gray, W. M. Global view of the origin of tropical disturbances and stoRMS. *Mon. Weather Rev.* **96**, 669–700 (1968).
43. DeMaria, M., Knaff, J. A. & Connell, B. H. A Tropical Cyclone Genesis Parameter for the Tropical Atlantic. *Weather Forecast* **16**, 219–233 (2001).
44. Zhao, H. et al. Decreasing global tropical cyclone frequency in CMIP6 historical simulations. *Sci. Adv.* **10**, eadl2142 (2024).
45. Riehl, H. *Tropical Meteorology*. vol. 392 (McGraw-Hill, 1954).
46. Michaelis, A. C. & Lackmann, G. M. Climatological Changes in the Extratropical Transition of Tropical Cyclones in High-Resolution Global Simulations. *J. Clim.* **32**, 8733–8753 (2019).
47. Vecchi, G. A. & Soden, B. J. Increased tropical Atlantic wind shear in model projections of global warming. *Geophys. Res. Lett.* **34**, 2006GL028905 (2007).
48. Camargo, S. J., Emanuel, K. A. & Sobel, A. H. Use of a Genesis Potential Index to Diagnose ENSO Effects on Tropical Cyclone Genesis. *J. Clim.* **20**, 4819–4834 (2007).
49. Carlson, T. N. Some remarks on African disturbances and their progress over the tropical Atlantic. *Mon. Weather Rev.* **97**, 716–726 (1969).
50. Cresswell-Clay, N. et al. Twentieth-century Azores High expansion was unprecedented in the past 1,200 years. *Nat. Geosci.* **15**, 548–553 (2022).
51. Galarneau, T. J., McTaggart-Cowan, R., Bosart, L. F. & Davis, C. A. Development of North Atlantic Tropical Disturbances near Upper-Level Potential Vorticity Streamers. *J. Atmos. Sci.* **72**, 572–597 (2015).
52. Shearman, R. K. & Lentz, S. J. Long-Term Sea Surface Temperature Variability along the U.S. East Coast. *J. Phys. Oceanogr.* **40**, 1004–1017 (2010).
53. Meiler, S., Ciullo, A., Kropf, C. M., Emanuel, K. & Bresch, D. N. Uncertainties and sensitivities in the quantification of future tropical cyclone risk. *Commun. Earth Environ.* **4**, 371 (2023).
54. Ritchie, E. A. & Elsberry, R. L. Simulations of the Extratropical Transition of Tropical Cyclones: Phasing between the Upper-Level Trough and Tropical Cyclones. *Mon. Weather Rev.* **135**, 862–876 (2007).
55. Evans, C. et al. The Extratropical Transition of Tropical Cyclones. Part I: Cyclone Evolution and Direct Impacts. *Mon. Weather Rev.* **145**, 4317–4344 (2017).
56. Keller, J. H. et al. The Extratropical Transition of Tropical Cyclones. Part II: Interaction with the Midlatitude Flow, Downstream Impacts, and Implications for Predictability. *Mon. Weather Rev.* **147**, 1077–1106 (2019).
57. Riahi, K. et al. The Shared Socioeconomic Pathways and their energy, land use, and greenhouse gas emissions implications: An overview. *Glob. Environ. Change* **42**, 153–168 (2017).
58. Guan, J., Yao, J., Li, M., Li, D. & Zheng, J. Historical changes and projected trends of extreme climate events in Xinjiang, China. *Clim. Dyn.* **59**, 1753–1774 (2022).
59. Yaddanapudi, R., Mishra, A., Huang, W. & Chowdhary, H. Compound Wind and Precipitation Extremes in Global Coastal Regions Under Climate Change. *Geophys. Res. Lett.* **49**, e2022GL098974 (2022).
60. Hersbach, H. et al. The ERA5 global reanalysis. *Q. J. R. Meteorol. Soc.* **146**, 1999–2049 (2020).
61. Mann, H. B. & Whitney, D. R. On a test of whether one of two random variables is stochastically larger than the other. *Ann. Math. Stat.* **18**, 50–60 (1947).
62. May, R. M. et al. MetPy: A Meteorological Python Library for Data Analysis and Visualization. *Bull. Am. Meteorol. Soc.* **103**, E2273–E2284 (2022).
63. Thorncroft, C. & Hodges, K. African Easterly Wave Variability and Its Relationship to Atlantic Tropical Cyclone Activity. *J. Clim.* **14**, 1166–1179 (2001).
64. Roberts, M. J. et al. Projected Future Changes in Tropical Cyclones Using the CMIP6 HighResMIP Multimodel Ensemble. *Geophys. Res. Lett.* **47**, e2020GL088662 (2020).
65. Sainsbury, E. M. et al. Can low-resolution CMIP6 ScenarioMIP models provide insight into future European post-tropical-cyclone risk? *Weather Clim. Dyn.* **3**, 1359–1379 (2022).
66. Alves, J. M. R., Miranda, P. M. A., Tomé, R. & Caldeira, R. Evolution of the subtropical surface wind in the north-east Atlantic under climate change. *Clim. Dyn.* **63**, 3 (2025).
67. Boucher, O. et al. Presentation and Evaluation of the IPSL-CM6A-LR Climate Model. *J. Adv. Model. Earth Syst.* **12**, e2019MS002010 (2020).
68. Volodin, E. et al. INM INM-CM4-8 model output prepared for CMIP6 CMIP piControl. Earth System Grid Federation https://doi.org/10.22033/ESGF/CMIP6.5080 (2019).
69. Tatebe, H. et al. Description and basic evaluation of simulated mean state, internal variability, and climate sensitivity in MIROC6. *Geosci. Model Dev.* **12**, 2727–2765 (2019).
70. Roberts, M. J. et al. Description of the resolution hierarchy of the global coupled HadGEM3-GC3.1 model as used in CMIP6 HighResMIP experiments. *Geosci. Model Dev.* **12**, 4999–5028 (2019).
71. Döscher, R. et al. The EC-Earth3 Earth system model for the Coupled Model Intercomparison Project 6. *Geosci. Model Dev.* **15**, 2973–3020 (2022).
72. Gutjahr, O. et al. Max Planck Institute Earth System Model (MPI-ESM1.2) for the High-Resolution Model Intercomparison Project (HighResMIP). *Geosci. Model Dev.* **12**, 3241–3281 (2019).
73. Danabasoglu, G. NCAR CESM2-WACCM model output prepared for CMIP6 CMIP historical. Earth System Grid Federation https://doi.org/10.22033/ESGF/CMIP6.10071 (2019).
74. Yukimoto, S. et al. MRI MRI-ESM2.0 model output prepared for CMIP6 CMIP. Earth System Grid Federation https://doi.org/10.22033/ESGF/CMIP6.621 (2019).
75. Seland, Ø et al. Overview of the Norwegian Earth System Model (NorESM2) and key climate response of CMIP6 DECK, historical, and scenario simulations. *Geosci. Model Dev.* **13**, 6165–6200 (2020).
76. Kelley, M. et al. GISS-E2.1: Configurations and Climatology. *J. Adv. Model. Earth Syst.* **12**, e2019MS002025 (2020).

Acknowledgements

This work is partially supported by the research project PID2023-146344OB-I00 (CONSCIENCE) financed by MICIU/AEI /10.13039/501100011033 and by FEDER, UE. This work is supported by the Interdisciplinary Mathematics

Institute of the Complutense University of Madrid. This work is also supported by the ECMWF Special Projects SPESMART and SPESVALE. C. Calvo-Sancho acknowledges the grant awarded by the Spanish Ministry of Science and Innovation - FPI program (PRE2020-092343). C. Calvo-Sancho acknowledges support from the GVA. PROMETEO Grant CIPROM/2023/38 and CSIC-LINCGLOBAL Ref. LINCG24042.

Author contributions

A.M.M. conducted the research, performed the analysis and drafted the article. C.C.S. contributed to the interpretation of the results and reviewed the article. J.J.G.A. contributed to the research and interpretation of the results and reviewed the article. J.D.F. reviewed the article. P.B. reviewed the article and contributed to the research. M.L.M. contributed to the research, supervised the work, reviewed the article, and contributed to the interpretation of the results. All authors have read and approved the final manuscript.

Competing interests

The authors declare no competing interests. The funding sponsors had no participation in the execution of the experiment, the decision to publish the results, or the writing of the manuscript.

Additional information

Supplementary information The online version contains supplementary material available at https://doi.org/10.1038/s41612-025-01317-0.

Correspondence and requests for materials should be addressed to A. Montoro-Mendoza.